Thermal Science and Engineering Progress 71 (2026) 104590

Contents lists available at ScienceDirect

Thermal Science and Engineering Progress

journal homepage: www.sciencedirect.com/journal/thermal-science-and-engineering-progress

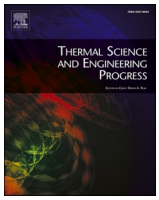

Conduction shape factors for thermal analysis of energy walls under varying boundary conditions

Aakash Gupta [a,*], Ida Shafagh [b], Simon Rees [a], Fleur Loveridge [a]

[a] School of Civil Engineering, University of Leeds, UK
[b] School of Mechanical Engineering, University of Leeds, UK

ARTICLE INFO

Keywords:
Energy geostructures
Shape factors
Heat exchangers
Geothermal energy
Energy walls

ABSTRACT

Embedded retaining walls in the buildings can be converted to energy walls by incorporating embedded heat exchanger pipes connected to a heat pump system, which can assist in decarbonising heating. To support the effective design of such systems, fast and reliable models are required to predict the thermal performance of energy walls. Analytical shape factors provide a convenient and computationally efficient method for estimating steady-state heat transfer rates within the wall. These shape factors are mathematical expressions that relate the temperature difference between surfaces to the resulting heat flux under steady conditions. While analytical shape factor equations have been successfully applied to other types of ground heat exchangers, their application and validations for energy walls, which have more complex thermal boundary conditions, remain unexplored. This study investigates the suitability of shape factor equations, originally developed for fuel transportation pipelines and other applications which share similar geometries, to the thermal analysis of energy walls. Given that energy walls may encounter varying thermal boundary conditions, e.g. air-exposed vs. fully embedded, both scenarios are analysed. The results present the first systematic parametric validation across realistic energy wall geometric variations (pipe spacing, diameter, wall thickness and cover depth) and thermal conductivity ratios to evaluate shape factors for practical design applications. The performance of analytical shape factors is benchmarked against results from steady-state and transient numerical models. The findings demonstrate that, with the developed methodology, existing shape factor equations can be successfully extended to energy walls and other energy geostructures exhibiting planar thermal behaviour.

1. Introduction

Reducing global dependence on fossil fuels is essential to address the climate emergency. Simultaneously, energy markets remain under stress due to ongoing global events. A transition to renewable energy is therefore necessary, both to significantly lower emissions and to enhance energy security.

Geothermal energy plays a key role in this transition, offering low air pollution and minimal environmental impact [1]. Among geothermal technologies, shallow geothermal systems, particularly those using heat pumps, are among the fastest-growing [2]. These systems can exploit thermal energy from shallow ground depth via energy geostructures: civil engineering structures in contact with the ground, integrated with ground source heat pumps [3]. In these systems, a heat pump is connected to a network of pipes embedded within subsurface structural elements. Thermally activating these elements, such as retaining walls, piles, or tunnels, can be accomplished during underground construction.

Amongst these energy geostructures, thermally activated retaining walls, known as energy walls, are a relatively recent innovation. Consequently, the development of reliable methods for their thermal analysis remains in the early stages [4]. This presents a challenge, as fast thermal analysis methods are needed to estimate energy availability and to integrate with building energy design models. Due to their large surface area, energy walls can accommodate a wide variety of heat transfer pipe configurations [5]. However, they also exhibit steep temperature gradients between the embedded pipes and the wall surfaces, both those in contact with the ground and those exposed to ambient air [6,7]. These complexities contribute to the current lack of analytical solutions for assessing the thermal performance of energy walls.

In energy geostructures, a much larger domain, the ground, surrounds a much smaller body or multiple bodies, energy geostructures,

* Corresponding author.
E-mail addresses: a.gupta5@leeds.ac.uk (A. Gupta), I.Shafagh@leeds.ac.uk (I. Shafagh), S.J.Rees@leeds.ac.uk (S. Rees), F.A.Loveridge@leeds.ac.uk (F. Loveridge).

https://doi.org/10.1016/j.tsep.2026.104590
Received 26 June 2025; Received in revised form 12 February 2026; Accepted 13 February 2026
Available online 16 February 2026

Nomenclature

Symbol	Description, Units
S_F	Shape Factor, Dimensionless
S_{GE}	Shape factor for GE energy Wall, Dimensionless
S_{GG}	Shape factor for part II in GG energy wall, Dimensionless
S'_{GG}	Shape factor for part I in GG energy wall, Dimensionless
S_{Rec}	Shape factor for part III in GG energy wall, Dimensionless
R	Thermal resistance, mK/W
q'	Heat Flux per unit length, W/m
q	Heat flux per unit area, W/m^2
λ	Thermal Conductivity, W/(mK)
ΔT	Temperature Difference, °C or K
T_p	Temperature at pipe wall, °C
T_W	Temperature at wall, °C
s	Pipe Spacing, m
D	Pipe Diameter, m
r_i	Pipe Radius, m
W	Wall thickness, m
c	Cover (pipe center to interface), m
c'	Net cover (pipe surface to interface), m
λ*	Thermal conductivity ratio (λ_S/λ_C), Dimensionless
λ_S	Soil/ground thermal conductivity, W/(mK)
λ_C	Concrete/wall thermal conductivity, W/(mK)

which needs to be thermally assessed. Compared to the much larger domain, the smaller domain can be assumed to have a steady nature [8]. Hence, in many studies of energy geostructures, the temperature field in the ground is generally solved through a transient approach (e.g. [9–12]) whereas the geostructure itself is assessed through a steady-state approach (e.g. [13,14]). This work focuses on the latter part, i.e. the steady-state.

A critical step in developing effective design methods is to understand how the geometry and thermal boundary conditions of the wall influence heat transfer, which is typically characterised through thermal resistance. Calculating the thermal resistance also enables rapid estimation of temperature differences across the geostructure for a given flux, an essential input for full thermal system design. One method of determining the value of a thermal resistance is by using a shape factor.

Despite many numerical studies examining the thermo-mechanical behaviour and long-term thermal performance of energy walls (e.g., [6,7,15]), there are still critical gaps in the literature: (1) No unified analytical framework exists for practitioners to rapidly estimate thermal resistance across varying geometries and boundary conditions, current methods require computationally expensive finite element analysis; (2) The applicability of shape factors (as commonly used for other ground heat exchangers) to planar energy wall configurations under varying thermal loads has not been extensively validated; and (3) A rigorous quantification of accuracy across realistic parametric variations (pipe spacing, wall thickness, thermal conductivity ratio) is lacking. This paper addresses these gaps.

While shape factors or thermal resistances have been successfully applied to energy piles [16–18] and borehole heat exchangers [14,19], their application to the energy walls presents unique challenges that have not been fully addressed in prior literature. Energy walls differ fundamentally from energy piles and boreholes in two main ways: (i) they have a planar rather than a cylindrical geometry, (ii) they exhibit two distinct thermal boundary condition scenarios (fully embedded, or exposed on one side), and in many cases, walls combine both conditions, which significantly affects their thermal resistance. Previous studies of energy walls employed numerical models but lacked analytical solutions compatible with rapid design assessment. This study addresses this gap by systematically validating shape factor equations across both energy wall configurations and performing parametric analysis on a range of geometric and material parameters.

Shape factors are a robust and well-established method for determining thermal resistance. They have been applied to energy geostructures [16–18] and are routinely used in the analysis of borehole heat exchangers [10]. This paper evaluates several approaches for calculating thermal resistance of energy walls using shape factors and proposes new recommendations for full thermal system design.

Section 2 provides background on shape factor theory and introduces the problem geometry. It then presents the development of modified shape factors, adapted from existing approaches and refined using analogies from electrical circuits. Section 3 introduces the numerical models, both steady-state variants and transient, that are used to benchmark the analytical predictions. Section 4 compares the results of these models with the proposed shape factors to assess their accuracy in predicting wall temperature differences. Section 5 discusses the broader applicability and limitations of the approach, and Section 6 concludes the study.

2. Shape factors for energy walls

2.1. Background

When heat is transferred within a body under steady-state conditions, a temperature field develops across the domain. Determining this temperature distribution typically involves solving second-order partial differential equations (PDEs) that must satisfy the boundary conditions of the geometry. However, obtaining exact analytical solutions is often challenging and time-consuming, and is limited to relatively simple geometries [20]. For more complex boundary conditions, numerical methods or approximate techniques, such as the integral method, scale analysis, and the use of shape factors, are commonly employed [21].

Among these, shape factors offer a simplified yet effective approach for estimating temperature differences between two surfaces under steady-state conditions [22]. They are widely used in the thermal analysis of borehole heat exchangers, where the relevant surfaces are typically the heat exchanger pipes and the borehole-ground interface [14,19,23]. Shape factors also provide valuable insight for design optimisation, such as pipe placements that enhance thermal performance. For instance, Jahanbin [24], demonstrated that cross-sectional geometries with higher shape factors yield improved heat transfer and, consequently, better coefficient of performance (COP).

In the context of this study, energy walls often exhibit repetitive pipe arrangements either vertically (Fig. 1a) or horizontally (Fig. 1b). These configurations can be idealised as unidirectional pipes embedded within a cuboidal wall (Fig. 1c), and further reduced to two-dimensional cross-sections, each containing a single circular pipe (Fig. 1d-e).

The resulting problem is thus reduced to calculating shape factors for steady-state (or quasi-steady-state) heat conduction in a cuboidal domain representing an energy wall of effectively infinite length, with equally spaced, eccentrically embedded, long cylinder pipes. While some energy walls may include dual pipelines (e.g. one on each face), the methodology developed in this study is expected to be extendable to such configurations.

Therefore, for the selected energy wall geometries under steady-state heat transfer, the relationship between the heat transferred per meter of wall or pipe length (q', W/m) and the temperature difference between the heat exchanger pipes and the wall surfaces (ΔT) can be expressed by Eq. (1).

$$q' = \lambda S_F \Delta T \tag{1}$$

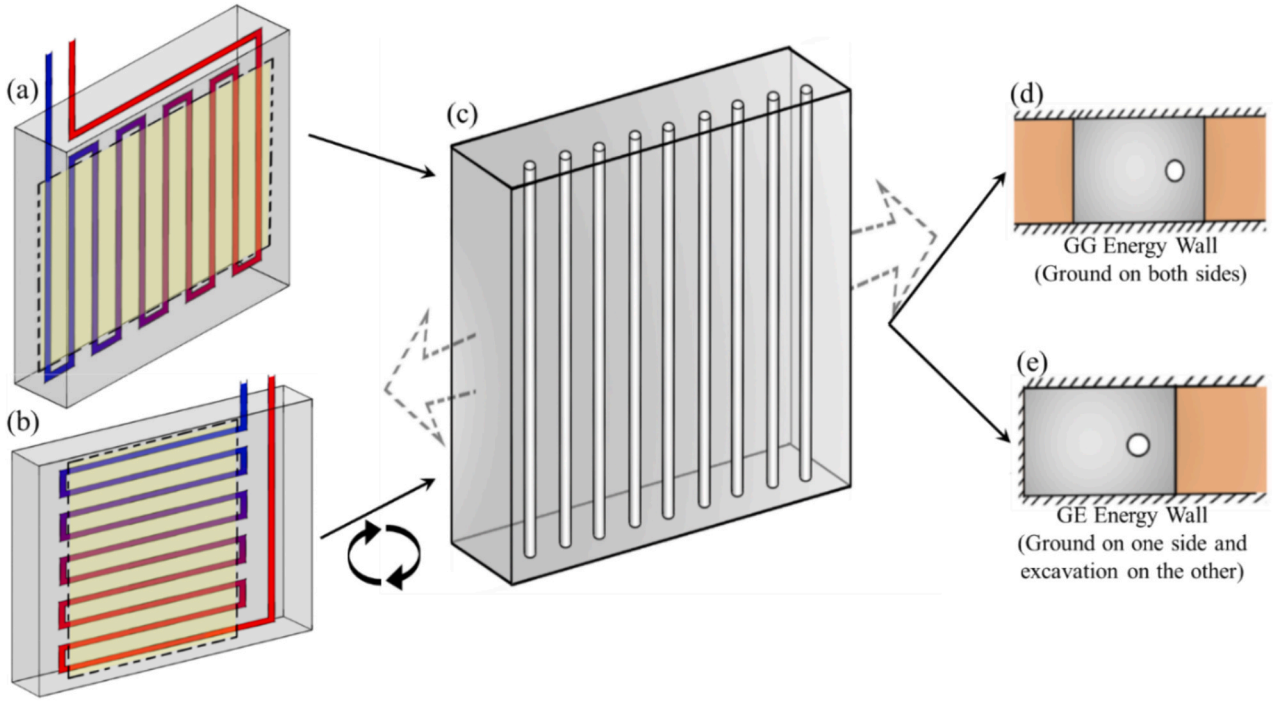

Fig. 1. Schematic representation of an energy wall with (a) vertical and (b) horizontal pipes arrangements. (c) Idealised as a geometry with equally spaced, repetitive embedded pipes. Two-dimensional cross-sections showing (d) a fully embedded (GG) configuration and (e) a configuration with one exposed side (GE).

where, S_F (dimensionless) is the shape factor, ΔT is the temperature difference and λ (W/(mK)) is the thermal conductivity of the wall material, typically concrete. Alternatively, this relation can also be expressed in terms of thermal resistance:

$$q'R = \Delta T, \cdot \text{where}, \cdot R = \frac{1}{\lambda S_F} \tag{2}$$

where R (mK/W) represents the thermal resistance of the wall. This formulation shows that heat transfer through the wall depends on two key components: the thermal properties of the material (through λ) and the geometry of the system (captured by the shape factor S_F).

While mathematically related through Eq. (2), shape factors and thermal resistances serve distinct conceptual roles. Thermal resistance (R) is a material and geometry-dependent property that defines the opposition to heat transfer. On the other hand, shape factors (S_F) are dimensionless geometric functions that enable a calculation of thermal resistance without solving the full differential equations. In the case of energy walls, the key innovation is that shape factors provide practitioners with explicit design equations (later through Eq. (3), Eq. (7) and Eq. (10) that directly give temperature predictions from known geometric and thermal parameters. This contrasts with existing approaches that require full numerical modelling. The shape factor formulations derived here are therefore not simply alternative expressions of thermal resistances, but rather analytical tools developed and validated specifically for energy wall configurations.

In the case of energy walls, the heat exchanger pipe is embedded within the wall, which is itself buried in the ground. A particular challenge in analysing energy walls is the presence of three surfaces at potentially different temperatures. While the two long sides of the wall (as shown in Fig. 1d and 1e) can be assumed adiabatic to reflect the repetitive geometry of the embedded pipes, three primary surfaces remain relevant: the pipe wall, the rear face of the wall (which interfaces with the ground), and the front face, which may be exposed to either the ground or to air, depending on the installation (see Fig. 1d and 1e).

Due to these differing boundary conditions, it is useful to categorise the thermal analysis into two typical cases:

(i) GG (Ground-Ground): Energy walls with ground contact on both sides of the wall (Fig. 1d).
(ii) GE (Ground-Excavation): Energy walls where one side is in contact with the ground (typically the pipe side) and the other interfaces with an excavation, often exposed to air (Fig. 1e).

2.2. Energy walls with excavation on one side (GE)

For energy walls with excavation on one side (GE), the idealised geometry is presented in Fig. 2a. In this configuration, the exposed face of the wall is assumed to be adiabatic. When this assumption is applied to the energy walls, it generally gives conservative results, as shown in the analysis by [5]], and is therefore an appropriate design approach. This assumption also reduces the GE case to a classical two-surface shape factor scenario, where only the temperatures of the pipe surfaces and the wall-ground interface are of interest.

For this geometry, shape factors originally developed for evaluating heat losses from large-diameter buried fuel transportation pipes [25,26] can be adapted. The shape factor for the GE configuration is given by Eq. (3) (see Fig. 2b):

$$S_{GE} = \frac{2\pi}{\ln\left(\frac{2s}{\pi D}\sinh\left(\frac{2\pi c'}{s}\right)\right)} \tag{3}$$

where s is the pipe spacing, D is the pipe diameter, c' is the net cover (the distance from the centre of the pipe to the wall-ground interface), as illustrated in Fig. 2b, and the condition $s > 1.5D$ must be satisfied. Eq. (3) is derived using the general formulation by Yovanovich [27], based on curvilinear coordinates. In its original application, the domain below the pipe was assumed to be infinite [28]. When adapted for energy walls, the surrounding ground is replaced by the concrete wall, and the temperature at the ground surface is substituted with the temperature at the exposed wall face, denoted as T_W.

Notably, Eq. (3) does not include the wall thickness (W) as a parameter. Despite this, an initial evaluation by Gupta et al. [29] found that the equation demonstrated good agreement with steady-state

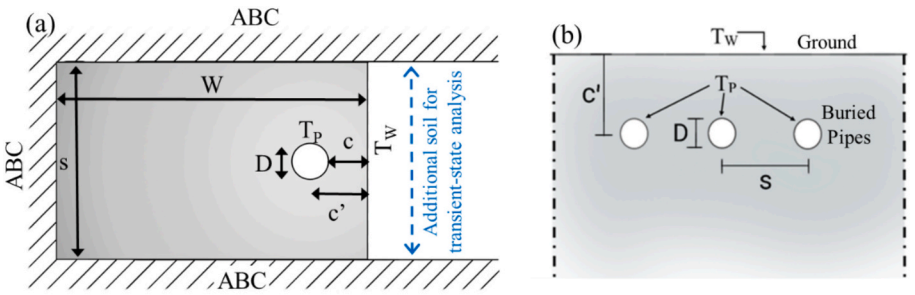

Fig. 2. Schematic representation of GE energy walls with one exposed side: (a) idealised geometry used for both conceptualisation and numerical simulation and (b) shape factor analogy based on buried pipe configurations. (W – wall thickness; s – pipe spacing; c – cover; c' – net cover; D – pipe diameter; T_p – Temperature at pipe boundaries; T_w – Temperature at wall/ground interface; ABC – adiabatic boundary condition).

numerical models across a range of pipe spacings and wall thicknesses. However, the approach was not tested for the full spectrum of relevant geometric configurations, particularly variations in pipe diameter, cover depth, and quasi-steady-state conditions, where the ratio of thermal conductivities between the wall concrete and the surrounding ground is also expected to influence results [18].

2.3. Energy walls with ground on both sides (GG)

In the case of fully buried energy walls (GG), heat transfer occurs across three surfaces: the pipe boundary, the wall face closest to the pipes, and the wall face farthest from the pipes (Fig. 3a). Unlike the GE configuration, a direct shape factor cannot be calculated here, as classical shape factor formulations are based on heat transfer between two surfaces only. However, an approximate shape factor can still be derived by analysing the flux distribution from the primary source (i.e. the pipes) to the two adjacent wall surfaces, which act as heat sinks [22].

In the current GG energy wall geometry, the pipe acts as the primary heat source or sink. Due to the repetitive arrangements of pipes, it is assumed that heat flux is symmetrically distributed, with exactly half transferring in each direction. The validity of the equal flux assumption is checked through a detailed examination of numerical results presented in Section 4.2, where the actual flux distribution is quantified and shown to remain within ± 2.2% of the equal split in the standard model. Accordingly, two separate shape factors can be defined to represent transfer toward each side of the wall. For simplification, and as illustrated in Fig. 3b, the region between the left half of the pipe and the wall surface further away is referred to as 'part I', while the region between the right half of the pipe and the adjacent wall surface is designated as 'part II'. Additionally, an additional section (the grey hatched region in Fig. 2b) of the hypothetical wall has been added to the geometry such that the pipe falls in the exact centre of the whole geometry, as shown in Fig. 3b, this region has been termed as Part III. The derivation of the shape factor for each region is presented in the following sections.

(i) Part I – Flux through furthest wall surface

For the wall surface farthest from the pipe (referred to as Part I in Fig. 3b), the shape factor formulation by Shafagh et al. [13] is used as the foundational equation. This model, illustrated in Fig. 4, is based on a geometry representing rows of pipes embedded within a wall.

$$S_e = \pi \left(\frac{1}{\ln\left(\frac{\sinh\left(\frac{\pi(b-e)}{2a}\right)}{\sinh\left(\frac{\pi r_i}{2a}\right)} \right)} + \frac{1}{\ln\left(\frac{\sinh\left(\frac{\pi(b+e)}{2a}\right)}{\sinh\left(\frac{\pi r_i}{2a}\right)} \right)} \right) \quad (4)$$

where e is the eccentric distance between the centre of the rectangular domain and the pipe, a and b are half of the pipe spacing and wall thickness, respectively, and r_i is the radius of the pipe. The equation is

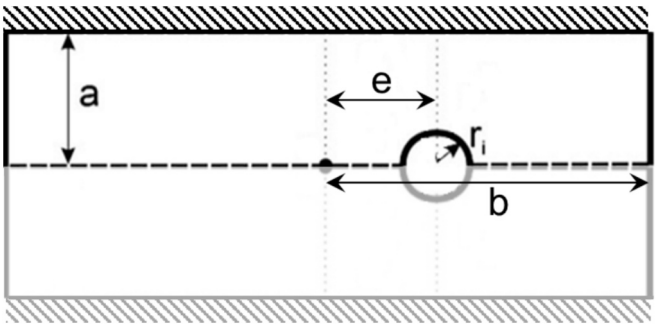

Fig. 4. Schematic representation of the pipe geometry used by Shafagh et al. [13] for deriving the shape factor (Eq. (4).

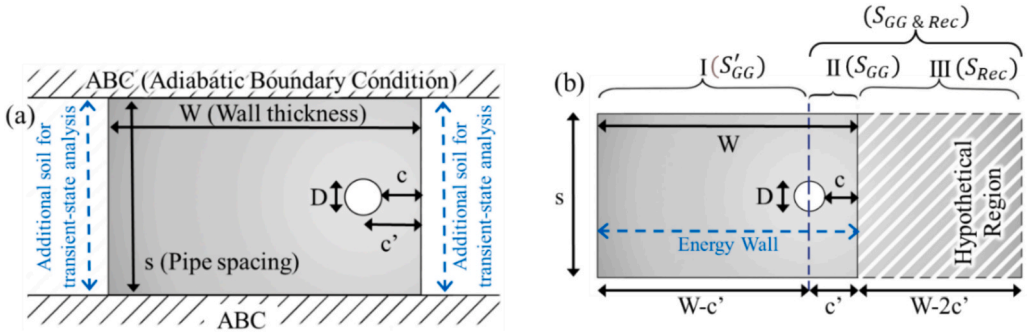

Fig. 3. Schematic representation of fully buried (GG) energy walls: (a) geometry used for both conceptual analysis and numerical simulation, and (b) is a wall with a pipe at the centre, which is divided into regions for the shape factor derivation, Shape factors S'_{GG}, S_{GG} and S_{REC} correspond to Parts I, II and III, respectively, Part III is hypothetical added for symmetry. (c- cover, c'- net cover, and D – pipe diameter).

derived assuming the pipe behaves as a concentrated heat source, with Dirichlet boundary conditions applied on both wall surfaces. While it accommodates eccentric placement of the pipe, the most accurate results are achieved when the pipe is centrally located (i.e., $e = 0$). When $e = 0$, Eq. (4) simplifies to:

$$S_{e0} = 2\pi \left(\ln \left(\frac{\sinh\left(\frac{\pi b}{2a}\right)}{\sinh\left(\frac{\pi r_i}{2a}\right)} \right) \right)^{-1} \tag{5}$$

This expression can represent the shape factor of the entire domain (Part I + II + III in Fig. 3b or the full domain in Fig. 4 when eccentricity, $e = 0$). The corresponding thermal resistance, R_{e0}, can be calculated using Eq. (2). Based on the electrical analogy for resistances in parallel and series [28,30]. The total resistance R_{e0} is the result of a parallel connection of two symmetrical halves (Parts I and II), as shown in Eq. (6):

$$\frac{1}{R_{e0}} = \frac{1}{R'_{GG}} + \frac{1}{R_{GG\&Rec}} \Rightarrow \frac{1}{R_{e0}} = \frac{2}{R'_{GG}}, since, R'_{GG} = R_{GG\&Rec} \tag{6}$$

This can be converted back to the shape factor using Eq. (2), resulting in the expression given in Eq. (7).

$$S'_{GG} = \frac{\pi}{\ln\left(\frac{\sinh\left(\frac{\pi(W-c')}{s}\right)}{\sinh\left(\frac{\pi D}{2s}\right)} \right)} \tag{7}$$

(ii) Part II − flux through the closest wall surface

The shape factor for heat transfer from the pipe to the wall surface adjacent to it (referred to as Part II in Fig. 3b) can also be determined using resistance relationships. According to Eq. (6), the thermal resistance of Part I is equal to the combined resistance of Part II and hypothetical Part III. The resistance for Part I, R'_{GG}, is already derived in Eq. (6). The shape factor of part III, denoted as S_{Rec}, can be calculated using the classical formulae for heat conduction between two opposite faces of a cuboid. This is given by Eq. (8) [31] and can be converted to thermal resistance using Eq. (2).

$$S_{Rec} = \frac{s}{W - 2c'} \tag{8}$$

Following the relationship $R'_{GG} = R_{GG\&Rec}$, where R_{GG} and R_{Rec} are in series [30]. The thermal resistance of Part II can be isolated as:

$$R_{GG} = R'_{GG} - R_{Rec} \tag{9}$$

This resistance can either be used directly or converted back to a shape factor using Eq. (2). Alternatively, the shape factors for Part II, S_{GG}, can be calculated from the shape factors of the other two parts using Eq. (10).

$$\frac{1}{\lambda S_{GG}} = \frac{1}{\lambda S'_{GG}} - \frac{1}{\lambda S_{Rec}} [LRDA] \frac{1}{S_{GG}} = \frac{1}{S'_{GG}} - \frac{1}{S_{Rec}} \tag{10}$$

The whole resistance network concept from Eqs. (6)–(10) relies on the assumption that thermal resistances can be treated as series and parallel components. This approximation is exact for cylindrical symmetry (as in e.g. borehole heat exchangers or energy piles) but approximate for planar multi-surface systems. The error introduced by this is discussed in Section 4.4.

Moreover, it is important to note that Eq. (7) and Eq. (10) must be applied separately to each part, as their thermal resistances differ depending on the distance from the heat source (i.e., the pipe). In practice, either S_{GG} or S'_{GG} is sufficient to determine the pipe wall temperature, provided the corresponding surface temperature is known. This implies that only one of the two shape factors is required for the thermal design of the energy wall. This simplification leads to several practical advantages, which will be discussed in the subsequent sections.

3. Numerical model and the parametric analysis

To evaluate the accuracy of the derived shape factors, S_{GE} (Eq. (3) for GE energy walls, and S'_{GG} (Eq. (7) and S_{GG} (Eq. (10), for GG energy walls, the results from these analytical expressions are compared against numerical simulations conducted across a range of geometric configurations. The numerical models are developed using COMSOL Multiphysics [32] for both GE and GG geometries, as depicted in Figs. 2a and 3a, respectively. Two types of simulations are carried out:

(i) steady-state simulations, allowing for direct comparison with analytical solutions.
(ii) transient simulations, which are run until quasi-steady-state conditions are reached and then compared with derived shape factors.

The simulation in COMSOL solves the heat diffusion equations, which govern the thermal behaviour of energy walls under both steady-state and transient conditions. Under steady-state conditions, where heat flux entering the system equals heat flux leaving and temperature profiles are time-invariant, the governing equation is:

$$\nabla^2 T = 0$$

where, T is the temperature, and the domain includes the concrete wall and the surrounding soil. Under transient (time-dependent) conditions, the governing equation is:

$$\rho c_p \frac{\delta T}{\delta t} = \lambda \nabla^2 T$$

where, ρ is the density (kg/m^3), c_p is the specific heat capacity (J/kg·K), t is time (s), and λ is thermal conductivity (W/(mK)). The numerical models are developed with the assumption that thermal properties are constant and do not change with temperature, and heat transfer is purely conductive. This is appropriate for the small temperature changes that will be experienced by energy walls made typically of low-permeability concrete. Additionally, since the pipe arrangements are repetitive, the lateral effects are assumed to be negligible, and the boundaries are applied with adiabatic boundary conditions. It should also be noted that the developed geometry under consideration is two-dimensional and therefore, longitudinal pipe variations along wall length (or depth) are neglected.

3.1. Model geometry and boundary conditions

Fig. 5 presents the geometry and boundary conditions applied in the numerical simulations. For GE energy walls, adiabatic boundary conditions are applied to the top and bottom edges of the model to represent the symmetric and repetitive nature of the embedded pipes. The exposed side is also assumed to be adiabatic, based on analysis by Makasis et al. [5], which showed this approach to be conservative for design purposes. This means that adopting a thermally insulated (adiabatic) boundary simulates the worst-case thermal performance. It assumes zero heat transfer through the energy walls, forcing the system to rely solely on the ground and concrete as its heat sinks. This predicts the highest fluid temperatures, ensuring the design is robust and not under-designed by relying on unrealistic heat leakage.

In the steady-state models, (Fig. 5a), the geometry does not include an extended ground domain. However, in the transient models (Fig. 5b), an extended ground region is included with a fixed far-field temperature (FFT) applied at its boundary. The domain size is selected to ensure that the far-field temperature does not influence the heat transfer within the energy wall. For GG energy walls, only transient simulations are

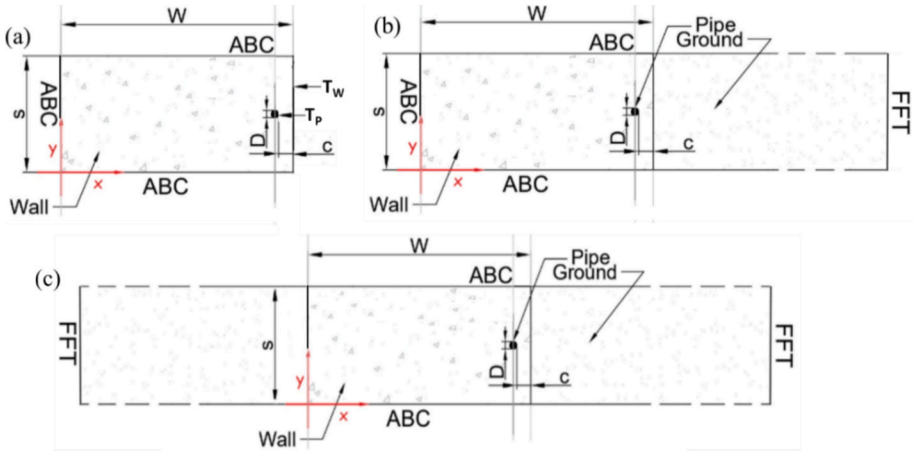

Fig. 5. Geometries used in numerical models: (a) GE-type energy wall for steady-state analysis, (b) GE-type for transient analysis, and (c) GG-type energy wall for transient analysis. ABC – Adiabatic Boundary Conditions; FFT – Far Field Temperature; W- wall thickness; s – pipe spacing; c – cover; D – pipe diameter.

conducted, using the geometry shown in Fig. 5c. In this case, the symmetry boundaries are treated as adiabatic, and a constant far-field ground temperature is applied at the outer boundary of the ground domain to simulate long-term thermal conditions.

To ensure solution accuracy, the mesh size was verified by progressive refinement, finalising on a minimum mesh element size of 0.0001 m to a maximum of 0.5 m mesh element size with a growth rate of 1.15. This provides a finer mesh near pipes and narrow regions. For transient analysis, time-step convergence was established by reducing time steps from 3600 s to 600 s, yielding temperature changes less than 0.01 °C at the initial 4–5 h, whereas having no difference at later time steps. Since the main region of study lies near the quasi-steady-state and quasi-steady state, where extremely small temperature changes occur over a period of days, therefore, it validates the 1-hour time-step as accurate. For steady state models, the flux from both pipe and wall surfaces is compared to check the flux balance. A similar procedure was adopted for transient state numerical models as well, with the results from standard models for GG discussed in Section 4.

For the steady-state analysis of GE Energy walls (Fig. 5a), temperature boundary conditions are applied to the pipe (T_P) and wall (T_W) boundaries. Because the system is in steady-state, the heat flux per meter, q' (W/m), entering and leaving the system should be equal. However, in COMSOL, the heat flux extracted from the walls and pipes is reported in units of W/m^2. Therefore, after simulation, the pipe heat flux q (W/m^2) and the wall surface heat flux q_W (W/m^2) can be compared using Eq. (11).

$$q' = q_W s = q\pi D \tag{11}$$

where s is the pipe spacing, and D is the pipe diameter. The heat flux q', derived from the steady-state numerical model, can be used along with the temperature difference between the pipe and wall surface, ΔT, to calculate the shape factor, S_F, using Eq. (12). This, in return, can be used to compute the thermal resistances, R, via Eq. (2).

$$q' = \lambda S_F \Delta T \Leftrightarrow S_F = \frac{q'}{\lambda \Delta T} \tag{12}$$

In the transient analysis of both GE and GG energy walls, a constant planar heat flux, $q_W = 2\pi$ W/m^2 (or 6.28 W/m^2) is applied for one year with a time step of 1 h, common to all models. When this heat flux is applied at the pipe boundaries, it must be converted to q using Eq. (11). This ensures consistent heat transfer across all modelsregardless of pipe spacing, cover or other physical parameters. Once a quasi-steady-state is reached, the temperature difference between the pipe and wall surface, along with the heat flux, is used to estimate the shape factor for GE energy walls (S_{GE}), and for GG energy walls (S_{GG} and S'_{GG}) using Eq. (9).

These shape factors are evaluated at the end of the simulation period, by which, all systems have reached quasi-steady-state conditions. In this study, a quasi-steady-state is defined as a condition where the temperature difference between the pipe and wall-ground interface changes by less than 0.01 °C over 720 h (30 days). A near-quasi-steady-state is defined as a change of less than 0.1 °C within the same period.

3.2. Parametric analysis

A parameter sensitivity analysis was conducted to assess the influence of key geometric parameters on the calculated shape factors. Numerical models were developed to evaluate the effect of variations in pipe spacing (s), wall thickness (W), pipe diameter (D), cover (c), and thermal conductivity ratio (λ*), as given in Table 1. The thermal conductivity ratio is defined as the thermal conductivity of soil/ground (λ_S) divided by the thermal conductivity of wall material (λ_C, typically concrete).

$$\lambda^* = \frac{\lambda_S}{\lambda_C} \tag{13}$$

The range of parameter values used in this study (see Table 1) was selected based on previous energy wall investigations [33–37], ensuring that realistic energy wall designs are encompassed. Extreme cases may be possible beyond these ranges, and therefore it would be recommended to conduct further verification in such circumstances. For each

Table 1
Standard model dimensions used for initial testing of both GE and GG Energy walls, along with the parameter variations applied in the sensitivity analysis.

Parameter	*In Standard Models*	*In Parametric Studies*
Pipe spacing (s)	*500 mm*	*300mm800mm*
Wall thickness (W)	*800 mm*	*500mm1000mm*
Pipe diameter (D)	*25 mm*	*20mm30mm*
Cover (c)	*75mms*	*50mm150mm*
Thermal Conductivity (λ) for ground (λ_S) and wall (λ_C)	*1 W/m/K*	*1.5 W/m/K* *2 W/m/K*
Density (ρ) for ground (ρ_S) and wall (ρ_W)	*2000 kg/m^3*	–
Heat Capacity (c_p) for ground (c_{pS}) and wall (c_{pW})	*800 J/kg/K*	–
Thermal conductivity Ratio (λ)*	*1.0 (λ_S = 1 W/m/K, λ_C = 1 W/m/K)*	*0.5 (λ_S = 1 W/m/K, λ_C = 2 W/m/K)* *1.0 (λ_S = 2 W/m/K, λ_C = 2 W/m/K)* *1.5 (λ_S = 1.5 W/m/K, λ_C = 1 W/m/K)* *2.0 (λ_S = 2 W/m/K, λ_C = 1 W/m/K)*

parameter, a base (standard) value was defined, along with corresponding lower and upper bounds used for the parametric analysis.

4. Results

The results of the analysis are presented in two stages. Sections 4.1 and 4.2 compare the temperature differences predicted using the shape factors from Section 2 with those obtained from numerical simulations of the standard model (Section 3, Table 1). Sections 4.3 and 4.4 then summarise the outcomes of the full parametric analysis, helping to define the range of conditions under which the shape factors remain applicable.

4.1. Temperature differences for exposed walls (GE)

For the standard model of GE energy walls, the shape factor S_{GE} (calculated using Eq. (3), would be 2.218, which, when converted to resistance (using Eq. (2), gives 0.451mK/W. When a heat flux of 2π W/m^2 is applied, the temperature difference between wall and pipe (through Eq. (12) becomes around 1.41 °C. For energy walls with exposed sides, the temperature difference between the pipe and the wall surface in the standard model is shown in Fig. 6. The transient analysis reveals a gradual increase in this temperature difference. A near-quasi-steady-state condition is reached after approximately 9 days, and full quasi-steady-state conditions are achieved around day 111. However, because a true steady state is not reached, the temperature difference continues to increase very slightly (< 0.01 °C in 30 days).

Fig. 6 also shows that the buried pipe analogy (using the shape factor S_{GE}, Eq. (3) is highly effective for exposed walls. The predicted temperature difference matches the steady-state numerical result within 0.005 °C, or 0.34%, for the standard case.

4.2. Temperature differences for embedded walls (GG)

For fully embedded walls, the entire wall geometry is divided into two sections (denoted as part I and part II in Fig. 3b) with separate shape factors applied to each section. For the standard model of GG energy wall, the shape factor for part I, S'_{GG} (Eq. (7) is approximately 0.50, which gives a resistance of approximately 2.01 mK/W (using Eq. (2), and a resulting temperature difference of 3.16 °C (using Eq. (12). On the other hand, for part II, S_{GG} (Eq. (10) is approximately 1.31, which in terms of resistance gives 0.76 mK/W (using Eq. (2) and a resulting temperature difference between the pipe and the wall surface of 1.19 °C (using Eq. (12).

The temperature difference between the pipe and each wall surface is calculated by assuming that half of the total heat flux is transferred through each surface. While the pipe temperature remains the same for both sides, the two wall surfaces are expected to exhibit different absolute temperatures. Accordingly, Fig. 7a presents results for the wall surface closest to the pipe, and Fig. 7b shows results for the wall surface furthest from the pipe.

Before evaluating the effectiveness of the shape factors, the validity of the assumption that the heat flux is evenly split between the two wall surfaces is examined using results from the numerical simulation. For the standard model, approximately 49.2% of the total heat flux passes through the wall surface closest to the pipe (part II in Fig. 3b), while 47.0% pass through the opposite surface (part I). Although these values do not sum exactly to 100%, the discrepancy (about 2.2%) is due to the system not being fully in steady state, owing to the continued thermal interaction with the surrounding soil mass. Nonetheless, the results suggest that equal flux division is reasonably valid.

Fig. 7a shows that the shape factor S_{GG}, (Eq. (10) estimates the temperature difference between the pipe and the nearby wall-ground interface with high accuracy within 0.0015 ℃ or 0.12% of the value predicted by the transient numerical model at quasi-steady-state. In Fig. 7b, the shape factor S'_{GG} (Eq. (7) estimates the temperature difference for the wall surface furthest from the pipe within 0.015 ℃ or 4.7% of the transient numerical result.

Moreover, Part II reaches a near-quasi-steady state in less than 4 h, whereas Part I requires 30 days to do so. A full quasi-steady-state is also achieved significantly faster at the wall surface closer to the pipe (within 3 or 5 days, as shown in Fig. 7a), compared to the wall surface farther from the pipe, which reaches this condition only after about 150 days (Fig. 7b). This discrepancy is due to the shorter heat transfer path and smaller surface area of Part II, which enables it to stabilise thermally much more quickly than Part I. These significantly different timescales for both sides to reach the near-quasi-steady state or quasi-steady state, part II within a few hours and part I over many weeks, reflect the different boundary conditions inherent to GG configurations compared with the direct application in the GE energy wall.

4.3. Shape factor sensitivity analysis, exposed walls (GE)

Fig. 8 presents the performance of the shape factor method for energy walls with exposed sides across a full range of parametric conditions. Analytical predictions are compared against both steady-state (SS) and transient-state (TS) numerical results. Consistent with findings from previous studies [7,38,39], Pipe spacing has the most significant effect on the absolute temperature difference, with closer pipe spacing improving thermal efficiency. In addition, reducing the cover depth (i.e. placing the pipes closer to the ground surface) also results in a lower temperature difference, enhancing overall performance.

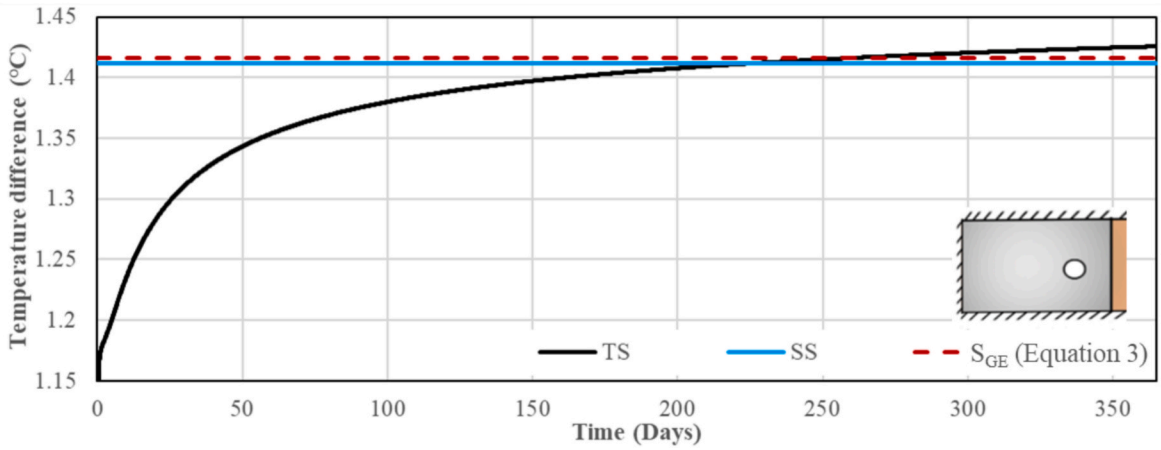

Fig. 6. Comparison of the temperature difference between the pipe and wall-ground interface for the standard model of exposed walls (GE), calculated using transient-state simulation (TS), steady-state simulation (SS), and the shape factor method (S_{GE})based on the buried pipe analogy (Eq. (3).

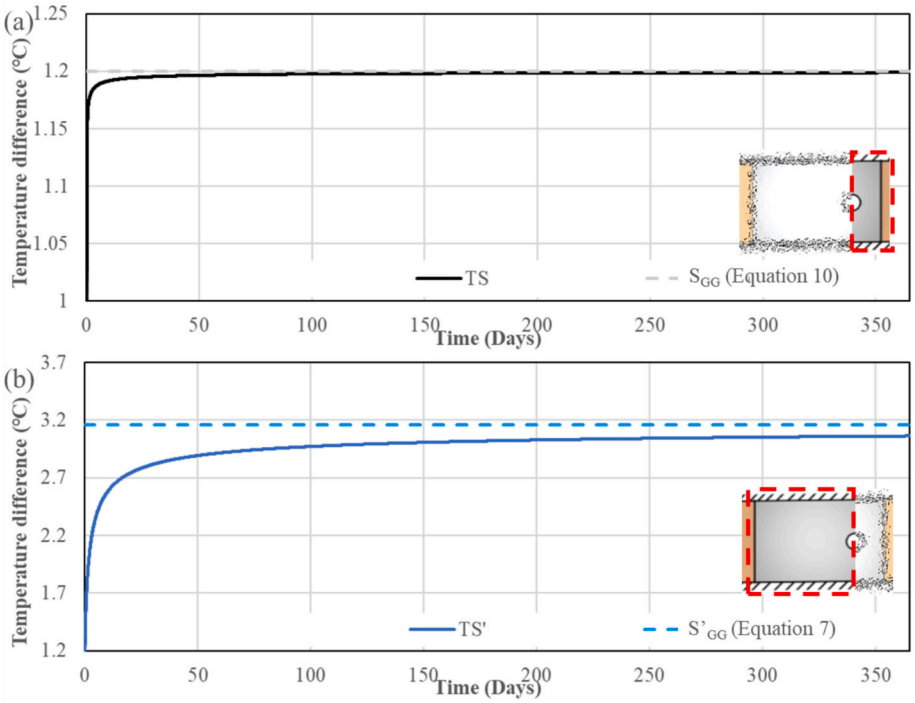

Fig. 7. Comparision of the temperature difference between the pipe and wall-ground interface predicted by the shape factors and transient state (TS) numerical simulations for (a) Part II, using S_{GG} (Eq. (10) and (b) Part I, using S'_{GG} (Eq. (7).

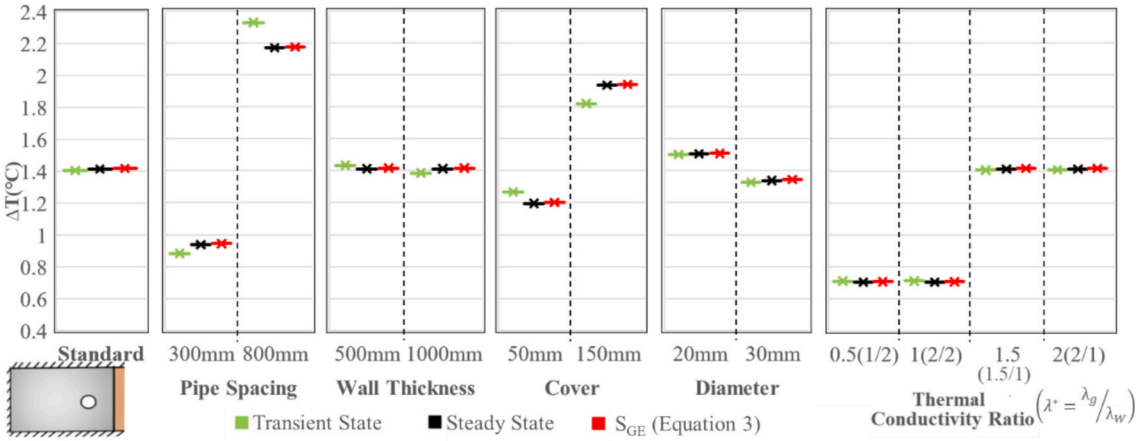

Fig. 8. Comparison of the temperature difference between the pipe and the wall-ground interface across a range of geometric conditions for the GE energy wall using the shape factor S_{GE} based on the buried pipe analogy (Eq. (3).

Overall, the temperature difference predictions using S_{GE} remain within 0.0073 ℃ (or 0.61%) across all cases. Minor variations are observed, primarily influenced by parameters included in Eq. (3) and how closely the wall geometry aligns with the buried pipe analogy. Accuracy improves with larger pipe spacing, as the buried pipe model, originally developed for widely spaced pipes to minimise thermal interface, is better approximated under such conditions. It is important to note that the buried pipe analogy does not account for wall thickness, assuming instead that the pipe is embedded in a semi-infinite medium (i.e. the ground). In contrast, energy walls have a finite and variable thickness, which introduces slight deviations in performance. Although Eq. (3) assigns the same shape factor regardless of wall thickness, small differences in temperature arise due to this variation. Interestingly, these differences are less significant than might be expected. As wall thickness increases, the wall's volume, and therefore the effective cross-sectional area, increases, which slows the approach to quasi-steady state in the numerical model. Nonetheless, for the typical range of wall thickness used in energy wall applications, the impact on temperature predictions remains negligible.

Additional variations observed in Fig. 8 are associated with changes in pipe cover. At lower cover values, the distance between the pipe boundaries and the wall surfaces is reduced. This leads to smaller temperature differences between the pipe and wall surfaces and results in quicker attainment of steady-state conditions. Conversely, at higher cover values, the time required to reach steady-state increases, which slightly reduces the temperature predictions, resulting in a maximum deviation of 0.61%. When the pipe diameter increases, the end-to-end spacing between adjacent pipes decreases. Since the cover remains constant, this effectively shifts the pipe centreline further from the wall-ground interface, slightly increasing the inaccuracy of the shape factor approximation to around 0.51%. In contrast, changes in the thermal conductivity ratio have no noticeable effect on the percentage error in

the shape factor predictions, indicating that the accuracy of the S_{GE} shape factor is largely independent of material conductivity differences within the tested range.

4.4. Shape factor sensitivity analysis, embedded walls (GG)

Fig. 9 presents the results from the parametric analysis for the wall surface closest to the pipe, while Fig. 10 presents the results for the wall surface farthest from the pipe. For temperature differences calculated using S_{GG}, where the pipes are adjacent to the wall surface, the predictions remain highly accurate, within 0.84% of the transient numerical solution (Fig. 9). However, for the case using $S'_{GG'}$, where the wall surface is farther from the pipes, the discrepancy increases, reaching up to 7% (Fig. 10). The largest deviation from the standard model occurs for S'_{GG} when the thermal conductivity ratio $\lambda^* = 2$, indicating that higher ground conductivity significantly affects how heat flux is distributed between the two wall surfaces. Specifically, greater conductivity in the surrounding soil reduces the proportion of flux reaching the outer wall surface (farther from the pipes), thereby lowering the accuracy of the shape factor prediction. When the thermal conductivity of ground and wall is more similar (i.e.$\lambda^* \sim 1$), the differences between analytical and numerical predictions are much smaller, remaining below 0.46% for the near-wall surface and under 6.5% for the far-wall surface.

5. Discussion

This work has systematically validated shape factor equations across various energy wall geometries, solving the issue of the steady-state response calculations for the energy walls. This can assist in better calculation of thermal resistances of the wall and hence improved design processes for energy walls. While the numerical models can predict thermal behaviour with high precision, they are computationally expensive and impractical for iterative design work. These validated shape factors presented here provide both speed and sufficient accuracy for integration into building energy design requirements. Overall, the shape factors developed for both GG and GE energy walls demonstrate strong agreement with the results of steady-state and transient-state numerical simulations conducted using COMSOL Multiphysics [32].

For GE energy walls, Eq. (3), based on the buried pipe analogy, consistently achieves very high accuracy, exceeding 99% in nearly all cases, while slightly underestimating the temperature values. This indicates that the shape factor can reliably predict temperature variations in the GE wall under constant or gradually varying thermal loads.

For GG energy walls, two distinct shape factors are available for estimating pipe temperatures. Since the design of energy walls ultimately requires the prediction of the fluid temperature, only one of these is actually required in the design process. Therefore, it is recommended to use the shape factor corresponding to part II (see Fig. 3a), i.e., S_{GG} from Eq. (10). This is because the region of the wall between the pipe and the adjacent wall-ground interface reaches a quasi-steady state within just a few hours after thermal activation. As a result, Eq. (10) can predict temperature variations with an error of less than 0.3%, making it suitable for both near-steady-state conditions and also varying thermal loads where the timescale of fluctuation is similar or larger than the steady state time.

On the other hand, if S'_{GG} is considered, the temperature at the far side is overpredicted by ~ 5%. If this is used in the total calculation, it cannot predict reliable temperature changes when the thermal load applied varies rapidly or in short-term behaviour. This is because under these conditions, the body would not reach a steady state, hence this overprediction by S'_{GG} using Eq. (7) would increase even more. Alternatively, in the case where the thermal load changes gradually, the final temperature difference would be slightly overestimated, which makes it useful. Therefore, for thermal scenarios involving rapid fluctuations or short-term cyclic behaviour (e.g., sub-hourly cycles), particularly those affecting the far side of the GG walls, truly transient models should be employed.

In summary, the temperature difference calculated via S_{GG} (using Eq. (10) is more reliable regardless of the timescale of load fluctuation and either S_{GG} (Eq. (10) and S'_{GG} (Eq. (7) can be used to predict temperature at pipe boundaries, S_{GG} should be preferred over S'_{GG}.

It is important to acknowledge that energy walls often consist of both embedded and exposed sections. To accommodate this, if the thermal response of the whole section is known, shape factors can be converted into thermal resistances (via Eq. (2) and combined using an electrical resistance analogy, weighted by the depth of each section. For example, if a uniform dimension wall is thermally activated, with a fully buried length of Y and an excavated length of X, they represent thermal resistance in series. The thermal resistance for the buried section, R_{GG} and the excavated section, R_{GE}, can be used to calculate the equivalent thermal resistance, R_{eq}, where $R_{eq} = \frac{YR_{GG}+XR_{GE}}{(X+Y)}$. . In this case, the equivalent shape factor, S_{eq}, would become $S_{eq} = \frac{(X+Y)S_{GE}S_{GG}}{YS_{GE}+XS_{GG}}$. Alternatively, as proposed by Sun et al. [33] and Rammal et al. [40], the thermal response of each section can be analysed separately, and the resulting temperatures averaged to estimate the outlet fluid temperature. A working example for this approach is presented in [41].

Additionally, the shape factors developed in this study assume that heat exchanger pipes are embedded on only one side of the energy wall. In some installations, particularly in embedded sections, pipes may be placed on both faces of the wall. While this configuration introduces additional complexity, the methods and principles presented here remain broadly applicable and can be adapted for further development in such cases.

Finally, the approach and shape factors proposed here may have

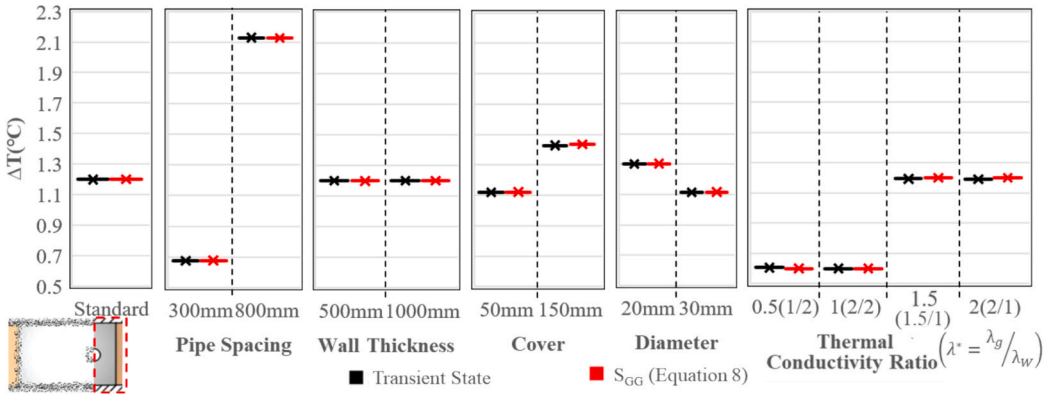

Fig. 9. Comparison of the temperature difference between the pipe and the adjacent wall-ground interface (part II) for various geometric configurations of the GG energy wall, using the shape factor S_{GG} (Eq. (10).

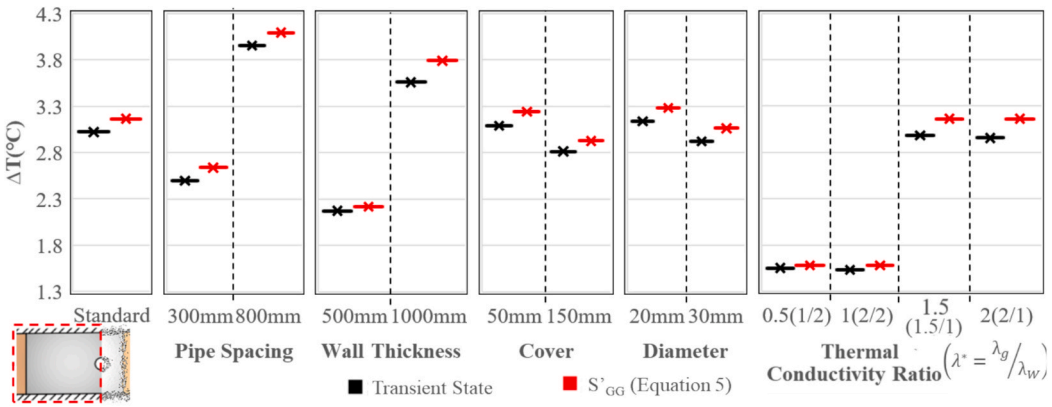

Fig. 10. Comparison of the temperature difference between the pipe and the wall-ground interface farther from the pipes (part I) for a range of geometric configurations of the GG energy wall using the shape factor S_{GG} (Eq. (7).

wider applications beyond energy walls. Similar planar heat transfer conditions arise in systems such as underfloor heating, thermally activated building systems (TABS), and pavement or bridge de-icing systems. As such, the analytical framework developed in this study offers a foundation for modelling and optimising a broader class of thermally active systems.

6. Conclusions

This study demonstrates the use of two-dimensional shape factors to calculate the thermal resistances of energy walls with varying geometries. These shape factors enable the prediction of temperature differences between the embedded heat exchanger pipes and the wall-ground interfaces under near steady-state thermal conditions. The shape factor for exposed energy walls, S_{GE}, is based on the analogy of equally spaced buried fuel pipelines, assuming the exposed surface to be insulated. In contrast, embedded energy walls require two shape factors, S'_{GG} and S_{GG}, to account for the two relevant wall surfaces, and these are developed using an electrical resistance analogy. The key conclusions drawn from this study are:

- For energy walls with an exposed surface, Eq. (3) predicts the temperature difference with high accuracy, with deviations of less than 0.6% from numerical results.
- For fully embedded energy walls, the shape factor, S_{GG} (Eq. (10) accurately estimates the temperature difference between the pipes and the wall surface, with an error margin of less than 0.1%.
- For both exposed energy walls and part II of embedded energy walls (i.e. the region between the pipe and the closest wall-ground interface), a quasi-steady state is reached rapidly. This indicates that shape factors S_{GE} and S_{GG} are suitable not only for steady-state but also for thermal loading scenarios where the load varies gradually with time.
- The shape factors have been validated across an array of realistic geometries, with excellent agreement observed between analytical predictions and numerical simulations for both wall types.

Therefore, this work advances the state-of-the-art in energy wall thermal design by providing shape factor equations which are systematically validated against all key parameters (pipe diameter, pipe spacing, wall thickness, cover, and thermal conductivity ratio), rather than giving solutions through isolated numerical models which have limited applications. This also provides solutions for both buried (GG) and exposed (GE) confidustaions, which make it easier for integration with other analytical models which assess the transient nature within soil. Therefore, this also provides practical design integration due to its high accuracy, making it reliable for adoption.

In summary, the shape factors presented in this work offer a reliable and efficient means of estimating temperature distributions within energy walls. Their integration could form a key component of a fully analytical design framework for energy wall systems, offering significant value when the thermal behaviour is known or when simplified yet accurate design tools are desired.

7. Data statement

Key data associated with this publication are openly accessible through the University of Leeds Research Data Repository [42].

CRediT authorship contribution statement

Aakash Gupta: Writing – review & editing, Writing – original draft, Visualization, Validation, Software, Methodology, Investigation, Formal analysis, Conceptualization. **Ida Shafagh:** Writing – review & editing, Visualization, Supervision, Methodology, Investigation, Formal analysis, Conceptualization. **Simon Rees:** Writing – review & editing, Supervision, Methodology, Conceptualization. **Fleur Loveridge:** Writing – review & editing, Visualization, Supervision, Resources, Methodology, Conceptualization.

Declaration of competing interest

The authors declare that they have no known competing financial interests or personal relationships that could have appeared to influence the work reported in this paper.

Acknowledgement

The Integrated Infrastructure for Sustainable Thermal Energy Provision (IN-STEP) project, grant reference EP/S001417/1, of the Engineering and Physical Sciences Research Council of the United Kingdom, provided funding for the work presented.

References

[1] I. Dincer, C. Acar, A review on clean energy solutions for better sustainability, Int. J. Energy Res. 39 (2015) 586–606, https://doi.org/10.1002/er.3329.
[2] L. Rybach, Global statusdevelopment and prospects of shallow and deep geothermal energy, Int. J. Terrestrial Heat Flow Appl. 5 (2022) 20–25, https://doi.org/10.31214/ijthfa.v5i1.79.
[3] A.A. Ahmed, M. Assadi, A. Kalantar, T. Sliwa, A. Sapińska-śliwa, A critical review on the use of shallow geothermal energy systems for heating and cooling purposes, Energies (Basel). 15 (2022) 1–22, https://doi.org/10.3390/en15124281.
[4] J. Zannin, A. Ferrari, P. Larrey-Lassalle, L. Laloui, Early-stage thermal performance design of thermo-active walls implemented in underground infrastructures, Geomech. Energy Environ. 30 (2020) 100218, https://doi.org/10.1016/j.gete.2020.100218.

[5] N. Makasis, G.A. Narsilio, A. Bidarmaghz, I.W. Johnston, Y. Zhong, The importance of boundary conditions on the modelling of energy retaining walls, Comput. Geotech. 120 (2020), https://doi.org/10.1016/j.compgeo.2019.103399.
[6] A. Coletto, D. Sterpi, Structural and geotechnical effects of thermal loads in energy walls, Procedia Eng. 158 (2016) 224–229, https://doi.org/10.1016/j.proeng.2016.08.433.
[7] D. Sterpi, A. Coletto, L. Mauri, Investigation on the behaviour of a thermo-active diaphragm wall by thermo-mechanical analyses, Geomech. Energy Environ. 9 (2017) 1–20, https://doi.org/10.1016/j.gete.2016.10.001.
[8] L. Laloui, A.F.R. Loria, Analysis and Design of Energy Geostructures: Theoretical Essentials and Practical Application, 2019.
[9] L.R. Ingersoll, O.J. Zobel, A.C. Ingersoll, Heat Conduction—With Engineering, Geological and Other Applications, Revised /, Oxford & lBH Publishing Co., New Delhi, 1969.
[10] G. Hellström, Ground heat storage: thermal analyses of duct storage systems, Lund University, 1991.
[11] N.R. Diao, H.Y. Zeng, Z.H. Fang, Improvement in modeling of heat transfer in vertical ground heat exchangers, HVAC and R Research 10 (2004) 459–470, https://doi.org/10.1080/10789669.2004.10391114.
[12] H. Brandl, Energy foundations and other thermo-active ground structures, Geotechnique 56 (2006) 81–122, https://doi.org/10.1680/geot.2006.56.2.81.
[13] I. Shafagh, S.J. Rees, F. Loveridge, Conduction Shape Factors for a Row of Equally Spaced Parallel Pipes Embedded Eccentrically in an Infinite Planar Structure, Unpublished Manuscript - Personal Communication with Ida Shafagh, School of Mechanical Engineering, University of Leeds, UK (n.d.).
[14] A.A. Koenig, Thermal resistance of borehole heat exchangers composed of multiple loops and custom shapes, Geotherm. Energy 3 (2015) 1–14, https://doi.org/10.1186/s40517-015-0029-1.
[15] N. Makasis, G.A. Narsilio, Investigating the thermal performance of energy soldier pile walls, Geomech. Energy Environ. (2021), https://doi.org/10.1016/j.gete.2021.100242.
[16] J. Claesson, S. Javed, Explicit multipole formula for the local thermal resistance in an energy pile-the line-source approximation, Energies (Basel). 13 (2020), https://doi.org/10.3390/en13205445.
[17] Z. Mohamad, F. Fardoun, F. Meftah, A review on energy piles design, evaluation, and optimization, J. Clean. Prod. 292 (2021) 125802, https://doi.org/10.1016/j.jclepro.2021.125802.
[18] F. Loveridge, W. Powrie, 2D thermal resistance of pile heat exchangers, Geothermics 50 (2014) 122–135, https://doi.org/10.1016/j.geothermics.2013.09.015.
[19] G.H. Go, S.R. Lee, S. Yoon, H. Park, S.K. Park, Estimation and experimental validation of borehole thermal resistance, KSCE J. Civ. Eng. 18 (2014) 992–1000, https://doi.org/10.1007/s12205-014-0454-x.
[20] K. Hirbodi, K. Jafarpur, A simple and accurate model for conduction shape factor of hollow cylinders, Int. J. Therm. Sci. 153 (2020) 106362, https://doi.org/10.1016/j.ijthermalsci.2020.106362.
[21] A. Bejan, A.D. Kraus, Heat transfer handbook, John Wiley & Sons Inc, Hoboken, New Jersey, 2003.
[22] W.M. Rohsenow, J.P. Hartnett, Y.I. Cho (Eds.), Handbook of Heat Transfer, Third, The McGraw-Hill Companies Inc, New York, 1975.
[23] S. Park, S. Lee, H.K. Park, S. Yoon, G. Go, H.B. Kang, J. Chung, An equivalent diameter in calculating borehole thermal resistance for spiral coil type GHE, in: The 2012 World Congress on Advances in Civil, Environmental, and Materials Research, Seoul, Korea, 2012, pp. 2508–2516.
[24] A. Jahanbin, Thermal performance of the vertical ground heat exchanger with a novel elliptical single U-tube, Geothermics 86 (2020) 101804, https://doi.org/10.1016/j.geothermics.2020.101804.
[25] H.H. Bau, S.S. Sadhai, Heat losses from a fluid flowing in a buried pipe, Int. J. Heat Mass Transf. 25 (1982) 1621–1629, https://doi.org/10.1016/0017-9310(82)90141-7.
[26] S. Chakraborty, Experimental investigation and modelling of heat loss mechanism from offshore buried Pipelines, Memorial University of Newfoundland (2017).
[27] M.M. Yovanovich, A general expression for predicting conduction shape factors, in: AIAA 11th Aerospace Sciences Meeting, American Institute of Aeronautics and Astronautics, Washington, D.C., 1973. https://doi.org/https://doi.org/10.2514/6.1973-121.
[28] Y.A. Cengel, A.J. Ghajar, Heat and mass transfer: fundamentals & applications, Fifth, McGraw Hill, New York, 2011.
[29] A. Gupta, F. Loveridge, I. Shafagh, S.J. Rees, Conduction Shape Factors for Thermally Active Retaining Walls, in: Symposium on Energy Geotechnics, Delft, Netherlands, 2023. https://doi.org/10.59490/seg.2023.535.
[30] A. Bhattacharyya, Heat Transfer Analogies, Stockholm, 1965.
[31] J.P. Holman, Heat Transfer, Tenth, McGraw Hill, New York, 2010.
[32] COMSOL, COMSOL Multipysics: Heat Transfer Module, User's Guide, © 1998–2018 Comsol (2015) 1–702.
[33] M. Sun, C. Xia, G. Zhang, Heat transfer model and design method for geothermal heat exchange tubes in diaphragm walls, 61 (2013) 250–259.
[34] S. Dong, X. Li, A. Minh, J. Michel, V.T. Nguyen, P. Che, Z. Xiong, Thermo-mechanical behavior of energy diaphragm wall: physical and numerical modelling, Appl. Therm. Eng. 146 (2019) 243–251, https://doi.org/10.1016/j.applthermaleng.2018.09.054.
[35] P. Bourne-Webb, S. Burlon, S. Javed, S. Kürten, F. Loveridge, Analysis and design methods for energy geostructures, Renew. Sustain. Energy Rev. 65 (2016) 402–419, https://doi.org/10.1016/j.rser.2016.06.046.
[36] I. Shafagh, F. Loveridge, Developing analysis approaches for energy walls, in: ICEGT 2020: E3S Web of Conferences, 2020: pp. 8–12. https://doi.org/10.1051/e3sconf/202020506005.
[37] A. Di Donna, F. Loveridge, M. Piemontese, M. Barla, The role of ground conditions on the heat exchange potential of energy walls, Geomech. Energy Environ. 25 (2021) 1–10, https://doi.org/10.1016/j.gete.2020.100199.
[38] A. Di Donna, F. Cecinato, F. Loveridge, M. Barla, Energy performance of diaphragm walls used as heat exchangers, Proceedings of the Institution of Civil Engineers: Geotechnical Engineering 170 (2017) 232–245. https://doi.org/10.1680/jgeen.16.00092.
[39] D. Adam, R. Markiewicz, Energy from earth-coupled structures, foundations, tunnels and sewers, Geotechnique 59 (2009) 229–236, https://doi.org/10.1680/geot.2009.59.3.229.
[40] D. Rammal, H. Mroueh, S. Burlon, Thermal behaviour of geothermal diaphragm walls: evaluation of exchanged thermal power, Renew. Energy 147 (2020) 2643–2653, https://doi.org/10.1016/j.renene.2018.11.068.
[41] A. Gupta, An analytical method to determine the amount of heat exchanged through thermally activated embedded retaining walls, University of Leeds, UK, 2024.
[42] A. Gupta, F. Loveridge, I. Shafagh, S. Rees, Data for - conduction shape factors for thermal analysis of energy walls under varying boundary conditions, University of Leeds, 2025, https://doi.org/10.5518/1782.